RSC Advances

Cite this: *RSC Advances*, 2012, **2**, 12670–12674

www.rsc.org/advances

COMMUNICATION

Defect-engineered $Si_{1-x}Ge_x$ alloy under electron beam irradiation for thermoelectrics†

Hyun Jung Kim,*[a] Hyung Bin Bae,[b] Yeonjoon Park[a] and Sang H. Choi[c]

Received 25th July 2012, Accepted 12th October 2012
DOI: 10.1039/c2ra21567e

We report the development of a defect-engineered thermoelectric material using $Si_{1-x}Ge_x$ alloys grown on a *c*-plane sapphire substrate *via* electron beam (E-beam) irradiation. This paper outlines the idea of growing the $Si_{1-x}Ge_x$ film at relatively high temperatures to obtain good crystalline properties, then controlling the amount of twins or dislocations through *ex situ* electron-beam irradiation. The current work suggests that structure reconstruction by bond rearrangement through E-beam irradiation may be used for tailoring thermoelectric properties.

The world's demand for energy is increasing dramatically, but current energy conversion systems run with only approximately 30% efficiency. One way to improve the sustainability of our energy requirements is the recovery of waste heat with thermoelectric (TE) generators. Thermoelectrics have long been too inefficient to be cost-effective in most applications; however, when the theoretical possibility of improving thermoelectric efficiency through nanostructural engineering was suggested in the mid-1990s, thermoelectrics came back under the spotlight. This revival of interest led to experimental efforts to fabricate new proof-of-principle and high-efficiency materials.[1–5] The efficiency of a thermoelectric material for both power generation and cooling is determined by its figure of merit (ZT): $ZT = S^2\sigma T/\kappa$, where S is the Seebeck coefficient, σ the electrical conductivity, κ the thermal conductivity, T the absolute temperature, and $S^2\sigma$ the power factor. As this equation indicates, the TE performance improves if the material intrinsically has a higher Seebeck coefficient, higher electrical conductivity, and lower thermal conductivity.

Glasses, because of their amorphous structures, exhibit some of the lowest lattice thermal conductivities. In a glass, thermal conductivity is viewed as a random walk of energy through one domain to another rather than rapid transport *via* lattice structure by phonons. This leads to the concept of a minimum thermal conductivity, κ_{min}. Actual glasses, however, make poor thermoelectrics because they lack the needed 'electron-crystal' property observed in crystalline semiconductors. Glasses have lower mobility due to increased electron scattering and lower effective masses because of broader bands. Good thermoelectrics are therefore crystalline materials that manage to scatter phonons without significantly disrupting the electrical conductivity. Thermoelectrics require a unique type of material property called 'phonon-glass electron-crystal'.[3,4,6] The electron-crystal property in crystalline semiconductors fulfils the required electronic properties such as Seebeck coefficient and electrical conductivity. $Si_{1-x}Ge_x$-based thermoelectric materials have been explored for over a decade as one of the most effective energy conversion materials at elevated temperatures. For applications at temperatures around 1000 °C, such as radioisotope thermoelectric generators (RTGs) used on NASA space missions since 1976,[7] $Si_{1-x}Ge_x$ alloys are among the known options.[6] $Si_{1-x}Ge_x$ alloys have an improved figure of merit because they maintain relatively high electrical conductivity and a lattice thermal conductivity which is lower than that of Si or Ge due to scattering of phonons by mass fluctuations and strain fields in the alloy.[8] Here, $Si_{1-x}Ge_x$ thin films have shown promising trends in performance from their ability to scatter phonons at stacking faults created by the 60° rotated primary twin structure. There exists a fundamental governing relationship in the rhombohedral epitaxy, *i.e.* the growth of cubic materials in the [111]-orientation on top of the basal *c*-plane of the trigonal sapphire crystals (Fig. S1†).

This work reports the development of a defect-engineered thermoelectric material using $Si_{1-x}Ge_x$ alloys grown on a *c*-plane sapphire substrate *via* electron beam (E-beam) irradiation. Electron and photon irradiation[9–11] have been suggested as alternative methods for crystallization, especially in isolated amorphous zones in semiconductors. For example, the sputtering and exchange of atoms by collisions with electrons from the beam was used to explain the formation and stability of fullerene molecules on graphitic surfaces.[12] E-beam irradiation is usually used for structural phase change or transformation of materials. The current work suggests that structure reconstruction by bond rearrangement through E-beam irradiation may be used for tailoring thermoelectric properties. Considering the previous results of $Si_{1-x}Ge_x$ films on sapphire substrates, we grew the $Si_{1-x}Ge_x$ film at a relatively low temperature in order to induce more twin boundaries and dislocations for phonon scattering.[13–15] However, the film morphology was so degraded that the Seebeck coefficient and electrical conductivity were reduced, resulting in the decrease of the TE figure of merit.[14] Instead, this paper provides a solution in which the $Si_{1-x}Ge_x$ film is grown at a

[a]*National Institute of Aerospace (NIA), 100 Exploration Way, Hampton, VA 23666, USA. E-mail: Hyunjung.Kim@NASA.Gov*
[b]*Korea Advanced Institute of Science and Technology KAIST, 291 Daehak-ro (373-1 Guseong-dong), Yuseong-Gu, Daejeon 305-701, Republic of Korea*
[c]*NASA Langley Research Center, Hampton, VA 23681-2199, USA*
† Electronic supplementary information (ESI) available: Crystal alignments, X-ray diffraction data, EDS spectra and Brillouin zones. See DOI: 10.1039/c2ra21567e

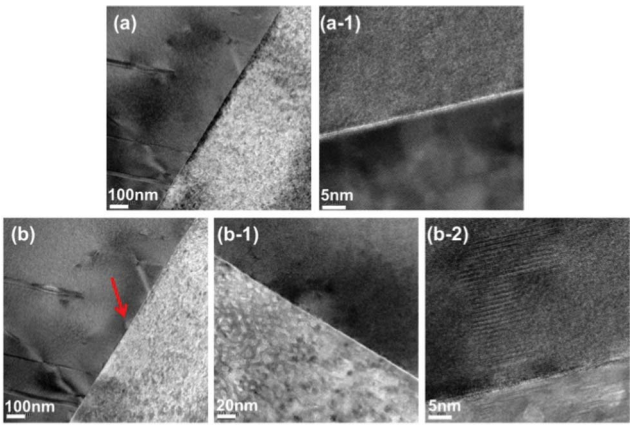

Fig. 1 Cross-sectional TEM images (at 195 K magnification) of the same site of a $Si_{1-x}Ge_x$ film (a) before and (b) after E-beam irradiation in a TEM for 1 h. The stacking faults were formed by the TEM beam for 1 h at the site marked with an arrow.

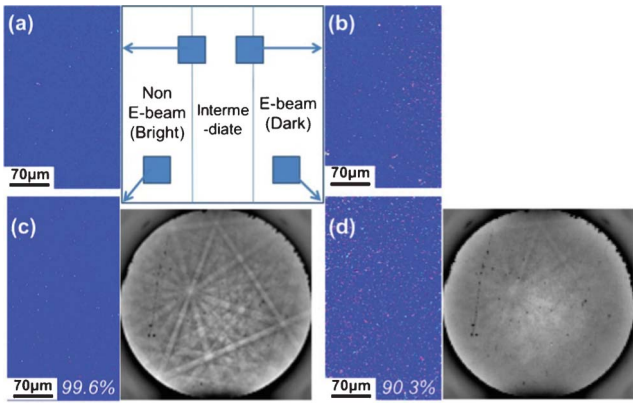

Fig. 3 EBSD results (a) and (b) at boundary of intermediate area, (c) at the area blocked from E-beam irradiation and (d) at the area exposed to the E-beam using a flood electron gun. The secondary electron diffraction patterns measured at one point in each side are attached.

relatively high temperature to obtain good crystalline properties, then the amount of twins or dislocations is controlled through *ex situ* electron-beam irradiation. This can maintain (or increase) the Seebeck coefficient and electrical conductivity. Also, this can introduce additional scattering of the lattice vibration phonon at defects such as embedded stacking faults, twins and dislocations.[16–20]

Two different electron beam sources were used for E-beam irradiation of the $Si_{1-x}Ge_x$ samples: one is a focused electron beam in a TEM and the second is a separate flood electron gun assembly. Fig. 1 shows a TEM bright field image and a high-resolution TEM image of the same site on a $Si_{1-x}Ge_x$ film (a) before and (b) after E-beam irradiation in the TEM for 1 h. There is no stacking fault at the interface between the $Si_{1-x}Ge_x$ film and the sapphire substrate before the E-beam irradiation in the TEM (Fig. 1(a-1)). After the E-beam irradiation in the TEM for 1 h, the stacking faults were clearly developed (Fig. 1(b-2)).

Using the flood electron gun assembly, half of the surface of a 99.6% single crystal $Si_{1-x}Ge_x$ sample (Fig. S2†) was irradiated for 1 h. Fig. 2 and 3 show the color-coded SEM images of this $Si_{1-x}Ge_x$ film with crystal orientation mapping as analyzed by electron backscatter diffraction (EBSD). There were three portions clearly shown in the two SEM images (Fig. 2(a)–(b)), which were evident even from the low magnification SEM image in Fig. 2(b). The left side of the image in Fig. 2(a) had no irradiation from the E-beam and appears slightly brighter, while the right side, which was irradiated by the E-beam, has a relatively dark surface. There is an intermediate portion between the bright and dark areas because diffracted electrons through the edge of a block have spread over a partially affected area. In Fig. 2(c), the EBSD results are represented by several line-art cubic shapes indicating the crystal orientation of each color domain. The same-colored domain indicates the same crystal orientation. A majority of the area is blue-colored and indicates a [111]-oriented single-crystal region. The EBSD image shows that long range order of the E-beam irradiated side on the right was reduced, which indicates a decrease in the amount of [111]-oriented crystals in that region of the sample. Quantitative analysis performed at higher magnification, shown in Fig. 3, reveals the ratio of [111]-oriented majority single-crystal region was decreased from 99.6% to 90.3% by E-beam irradiation.

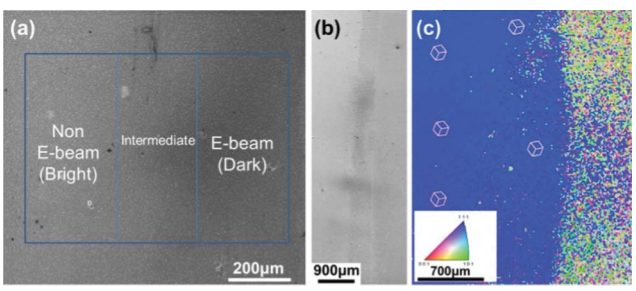

Fig. 2 (a) SEM image at 0° tilt; (b) low magnification SEM image at 70° tilt; (c) color-coded SEM images of a $Si_{1-x}Ge_x$ film with crystal orientation mapping as analysed by EBSD. The left half of the sample shown is the as-grown $Si_{1-x}Ge_x$ and the right half of the sample was E-beam irradiated using a flood electron gun.

During E-beam irradiation, bonding structures of the $Si_{1-x}Ge_x$ crystal break down and leave dangling bonds mostly at the surface. Such a disordered structure not only appears at the surface, but also deep below the surface due to repeated high-energy electron collisions. The energy transfer from the electrons to the sample causes bond breakage and subsequently creates short/long range disorder as shown in the EBSD images.

Fig. 4 shows TEM bright field images of the sample before (left side) and after (right side) E-beam irradiation with a flood electron gun. More twins and dislocations were formed by the E-beam irradiation. The change of morphology will also affect the electrical conductivity since the mobility is related to the surface coverage and film connectivity. The increase of the mobility (electrical conductivity) of the flat film was explained by more uniform substrate coverage than island growth.[21] Although the central part of the image in Fig. 4(b) was excessively removed by a milling process using the focused ion beam (FIB), we can speculate that the morphology of the film was maintained by considering that the remaining protection layer was flat as indicated by the arrow shown in Fig. 4(b). Also, there was no noticeable morphological change in the SEM images in Fig. 2(a) and (b). On the other hand, more twins (stacking faults) and dislocations were introduced in the flat film, which was originally a single crystal.

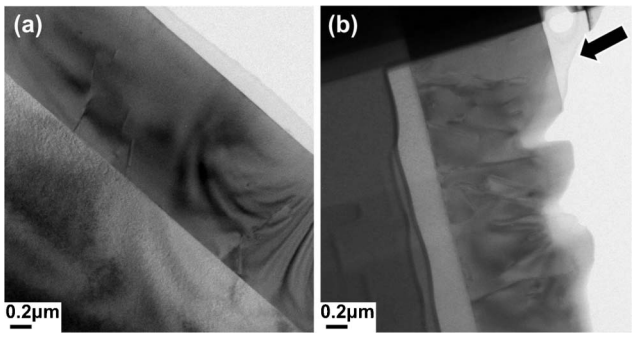

Fig. 4 Cross-sectional TEM images of an area (a) without E-beam irradiation and (b) irradiated with a beam current of 0.427 A for 1 h with a flood electron gun. The arrow confirms the morphology of the film was maintained after E-beam irradiation by considering that the film of the part of the protecting layer that remained was flat.

The Seebeck coefficient, $S = \Delta V/\Delta T$, is an intrinsic material property which describes the electrical potential (ΔV) associated with the given temperature difference (ΔT) in a material. The Seebeck coefficient is affected by the transport properties of charge carriers and is thus sensitive to impurities, defects, and phase transformation in materials. Experimentally, a single data point of the Seebeck coefficient can be obtained by measuring the temperature of two locations on a sample, and simultaneously measuring the voltage across these locations. Fig. 5(a) shows the scanned Seebeck coefficient data. The value of the Seebeck coefficient is shown in various colors, with corresponding values shown in the color chart. The Seebeck coefficient of the $Si_{1-x}Ge_x$ film is increased by about 10 μV K^{-1} by E-beam irradiation in Fig. 5(b). The similar sized, engineered structures with E-beam irradiation may decouple the Seebeck coefficient and maintain the electrical conductivity due to electron filtering[14,22] by selective emission of hot electrons that could result in a high power factor. Fig. 5(c) illustrates the temperature dependence of the Seebeck coefficient for a 4.1 × 10^{19} atoms cm^{-3} boron-doped $Si_{1-x}Ge_x$ film on *c*-plane sapphire before and after E-beam irradiation. This effect can be explained by the relocation and reformation process of dislocation patterns caused after the impact energy distribution of electrons, eventually causing the increase in the Seebeck coefficient. This increase may be understood from eqn (1). The Seebeck coefficient, *S*, is calculated using the following expression for each individual sub-band, *i*:

$$S = \sum_i \frac{1}{(eT)}\left[\frac{\langle E\tau\rangle}{\langle\tau\rangle} - E_f\right]_i \quad (1)$$

The value of the relaxation time $<\tau>$ decreases with increasing dislocation density.[16,23,24] At the end, the Seebeck coefficient increases with the bond potential that is proportional to the dislocation density and associated with domain-constricted scattering frequency. The observed increase shown in Fig. 5(b) and 5(c) correlates the dislocation scattering with increasing the entropy of randomness associated with the charge carrier flow within the system, leading in turn to an increase in the Seebeck coefficient.[23]

The high carrier mobility of single crystal $Si_{1-x}Ge_x$ improves the efficiency of thermoelectric devices since the electrical conductivity (σ) and electrical resistivity (ρ) are related to carrier concentration (n) through the carrier mobility μ: $1/\rho = \sigma = ne\mu$. Although twin lattice structures, dislocations and stacking faults are formed by E-beam irradiation, measurements revealed that the doping concentration and electrical conductivity of the portion exposed to E-beam

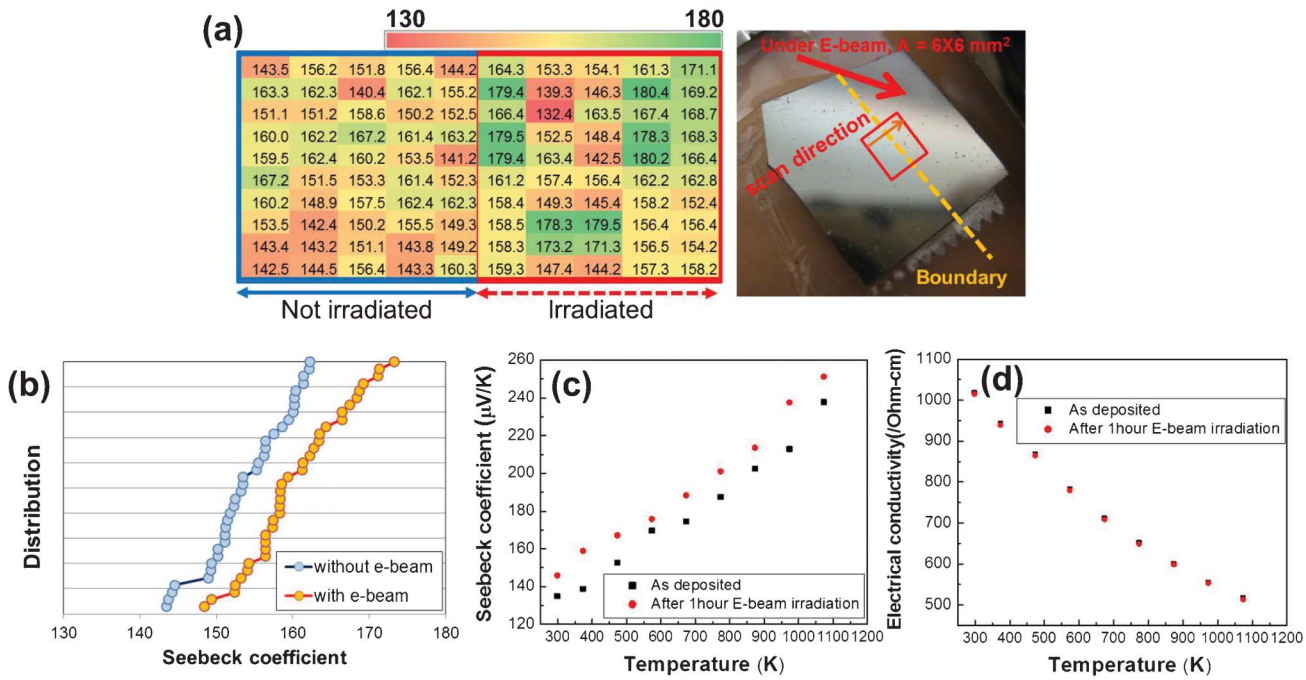

Fig. 5 (a) Scanned Seebeck coefficient (dimension: μV K^{-1}) measured results processed at room temperature. The electron beam was exposed on a half surface (right side) of the $Si_{1-x}Ge_x$ sample for 1 h. The photographic image shows the actual sample. (b) Distribution in the range of 15% to 85% of results (a) to remove measurement error. (c) Seebeck coefficient with elevated temperature of $Si_{1-x}Ge_x$ samples (dark squares: without E-beam, red circles: with E-beam). (d) Electrical conductivity with elevated temperature of $Si_{1-x}Ge_x$ samples (dark squares: without E-beam, red circles: with E-beam).

irradiation are not different from those values without E-beam irradiation. The sample alloy $Si_{1-x}Ge_x$ with heavy p-doping shows high electric conductivities of σ = 1018 Ω cm^{-1} (before E-beam irradiation) and 1015 Ω cm^{-1} (after E-beam irradiation) at 300 K. For both cases, the doping concentration for the former was 4.1 $\times$ 10^{19} atoms cm^{-3} and the latter was 3.8 $\times$ 10^{19} atoms cm^{-3}. The measured electrical conductivities of $Si_{1-x}Ge_x$ are between the values for single crystalline p-type Si and single crystalline p-type Ge. These data indicate that the electrical conductivity of defect-engineered $Si_{1-x}Ge_x$ with electron beam irradiation can also be comparable to single crystalline $Si_{1-x}Ge_x$. Fig. 5(d) shows the temperature dependency of the electrical conductivity. The increase of x (Ge concentration ratio) from 0.85 (before E-beam irradiation) to 0.88 (after E-beam irradiation) was confirmed by the $Si_{1-x}Ge_x$ profile obtained from energy-dispersive X-ray spectroscopy (EDS) measurements of TEM (Fig. S3†). The charge mobility of Ge is two to three times higher than that of Si, and even more if slightly strained.[25] The similar electrical conductivity with single crystal $Si_{1-x}Ge_x$ film after the E-beam irradiation can be explained by the composition ratio change along with the defect formation.

Defects suppress κ_{ph}, the phonon contribution to κ.[26] The thermal conductivity of the single crystal $Si_{1-x}Ge_x$ film is dominated by the phonon-Umklapp scattering (Fig. S4†), along with alloy scattering and scattering from the doping-impurities within the barriers, as is usual in semiconductors except in the limit of very high carrier concentrations. Although, including the electronic contribution to the thermal conductivity, it only plays a minor role.[23] It is clear from the structural analysis shown in Fig. 1 through 4 that our $Si_{1-x}Ge_x$ film has a high density of defects after E-beam irradiation. The defects introduce additional interfaces and cause the phonon scattering by phonons whose mean free path λ_{mfp} is much larger than the spacing between defect planes throughout the temperature range. By inserting defects during or after growth, more phonons can be scattered.

In summary, the power factor can be increased by appropriately engineering the defect structures (stacking faults, twins and dislocations) of the $Si_{1-x}Ge_x$ film. This communication introduces a new way to increase the power factor by growing the $Si_{1-x}Ge_x$ film at a relatively high temperature for the single crystalline properties and subsequently controlling the amount of twins or dislocations through *ex situ* electron-beam irradiation. The E-beam irradiated $Si_{1-x}Ge_x$ film enables a new and high performance TE material structure with a partially ordered and [111]-oriented continuous crystal layer. This TE material keeps not only high charge mobility for high electric conductivity without many grain boundaries, but is disordered enough to scatter propagating phonons in off-vertical directions at defects. Exploiting this control over the crystal structure can help synthesize defect-engineered films whose lattices have aperiodic arrays of twins along the growth direction (longitudinal) and lateral direction that modify phonon behavior by scattering the lattice vibration-phonon with embedded stacking faults and twin crystals. The electron transport property within the modified domain is almost unaffected. Although the dislocation scattering has a weak impact on both electrical and thermal transport properties, the critical factor is the ratio of the electrical to the thermal conductivity as compared to the Seebeck coefficient. The Seebeck coefficient of $Si_{1-x}Ge_x$ is increased after the E-beam irradiation by decreasing the relaxation time with increasing dislocation density due to E-beam irradiation. The volume of defects at the phonon scattering site can be controlled by adjusting the E-beam irradiation method (*in situ* or *ex situ*), current density and pulse time of the E-beam irradiation. However, an additional study for estimating the contribution to thermal conductivity by defects is needed, for example, the Callaway model.[27,28]

Experimental

Fabrication of $Si_{1-x}Ge_x$ film

A 99.6% single crystal $Si_{1-x}Ge_x$ film was grown at a growth temperature of 890 °C, a 5 sccm of high-purity argon gas, and using a 5 mTorr chamber pressure.[15]

E-beam irradiation

E-beam irradiation was carried out by two methods: (1) irradiation by TEM focused beam (Tecnai G2 F30, 300 kV, SA mode 195 K magnification, 1 h) on FIB's TEM sample and (2) irradiation by flood electron gun assembly (Kimball Physics Inc. models EGF-6115 and EGPS-6115) on a large area of $Si_{1-x}Ge_x$ film. For the second experiment, the electron beam was exposed on a half surface of the $Si_{1-x}Ge_x$ sample for 1 h. The beam voltage was set to 10 kV, giving a beam current of 0.427 mA (and filament = 1.337 V/4.257 A, 1st anode = 250 V).

Characterization of films

The crystal structure of the $Si_{1-x}Ge_x$ thin film was characterized using TEM (FEI, Tecnai G2 F30, 300 KV) and an EBSD detector (Hikari CCD detector). The surface morphology was measured using SEM (FEI, Nova230). The TEM sample was prepared using FIB (FEI, Quanta 3D FEG).

Electrical properties

Hall hole concentration and electrical conductivity are measured at room temperature with a Hall effect measurement system (EGK, HEM-2000).

Seebeck coefficient properties

[1] Scanning Seebeck coefficient measurement system: the Seebeck coefficient for samples with and without electron beam irradiation was measured using a scanning Seebeck coefficient measurement system used to directly detect local variations of the Seebeck coefficient on the film.[29] The scanned area was 6 mm $\times$ 6 mm with a data point interval of 600 μm. The average temperature of the sample was ~47 °C and ΔT was 21 °C. The larger the temperature difference created, the better the accuracy because it causes large ΔV, and this reduces voltage reading error. Thermocouple junctions were made with fine copper and constantan wires (T-type) with diameters of about 0.003″, and copper wire was used as a lead for the voltage reading.

[2] A high temperature apparatus for measurement of the Seebeck coefficient: the Seebeck coefficient was measured with a hand-built sample holder made from a machinable ceramic (model #960-15, Cotronics Corp.) along with custom-designed software. Two S-type thermocouples made of 0.003″ diameter wires of pure platinum and platinum/rhodium (10%) (Alfa Aesar Inc.) were used to measure the temperature and voltage difference of the $Si_{1-x}Ge_x$ film in the ~1 $\times$ 10^{-5} Torr vacuum chamber. The Seebeck coefficients were measured

from room temperature to 1100 K in 100 K increments. There is a specific description of the measurement system in ref. 14. To reduce errors, the same materials constructing the probe lines and probes were used.[14] For the Seebeck coefficient measurement system, we needed to introduce a correction factor because there are more errors in absolute temperature measurements at high temperature. In general, it is very difficult to measure the 'absolute temperature' of a sample surface at high temperature, especially in a vacuum. The correction factor is determined by comparing the Seebeck coefficient of a molybdenum sheet reported in the *CRC Handbook of Thermoelectrics*, with what we actually measure in the setup.[6] By introducing a correction factor from the test of standard materials, the deviation of the measured data from the known values could be adjusted. The correction factor, $y_{cor} = (3.945 \times 10^{-9})x^3 + (1.1039 \times 10^{-5})x^2 + 0.00428x - 0.5843$, was applied after the test.

Acknowledgements

This research was supported by a collaborative agreement between the NASA Langley Research Center and Federal Highway Administration, Department of Transportation under the inter-agency agreement #IA1-1098. The authors appreciate the assistance of Mr Tae Woo Lee and Mr Young Hoon Ha, FIB/SEM researchers at KAIST, South Korea.

Notes and references

1 M. S. Dresselhaus, G. Chen, M. Y. Tang, R. G. Yang, H. Lee, D. Z. Wang, Z. F. Ren, J.-P. Fleurial and P. Gogna, *Adv. Mater.*, 2007, **19**, 1043.
2 G. Chen, M. S. Drresselhaus, G. Dresselhaus, J.-P. Fleurial and T. Caillat, *Int. Mater. Rev.*, 2003, **48**, 45.
3 T. Tritt, Recent Trends in Thermoelectric Materials Research I, *Semiconductors and Semimetals*, Elsevier, 2001.
4 G. S. Nolas, J. Poon and M. Kanatzidis, *MRS Bull.*, 2006, **31**, 199.
5 S. M. Kauzlarich, S. R. Brown and G. F. Snyder, *Dalton Trans.*, 2007, 2099.
6 D. M. Rowe, *CRC Handbook of Thermoelectrics*, CRC press, Boca Raton 1995.
7 C. Wood, *Rep. Prog. Phys.*, 1988, **51**, 459.
8 J. P. Dismukes, L. Ekstrom, E. F. Steigmeier, I. Kudman and S. S. Beers, *J. Appl. Phys.*, 1964, **35**, 2899.
9 I. Jencic, E. P. Hollar and I. Robertson, *Philos. Mag.*, 2003, **83**, 2557.
10 M. Kaiser, L. van Pieterson and M. A. Verheijen, *J. Appl. Phys.*, 2004, **96**, 3193.
11 Z. W. Xu and A. H. W. Ngan, *Philos. Mag.*, 2004, **84**, 719.
12 T. Fuller and F. Banhart, *Chem. Phys. Lett.*, 1996, **254**, 372.
13 Y. Park, G. C. King and S. H. Choi, *J. Cryst. Growth*, 2008, **310**, 2724.
14 H.-J. Kim, Y. Park, G. C. King, K. Lee and S. H. Choi, *MRS Bull.*, 2011, **14**, 1314.
15 H. J. Kim, H. B. Bae, Y. Park, K. Lee and S. H. Choi, *J. Cryst. Growth*, 2012, **353**, 124.
16 J. R. Watling and D. J. Paul, *J. Appl. Phys.*, 2011, **110**, 114508.
17 D. Kotchetkov, J. Zou, A. A. Balandin, D. I. Florescu and F. H. Pollak, *Appl. Phys. Lett.*, 2001, **79**, 4316.
18 F. L. Madarasz and P. G. Klemens, *Int. J. Thermophys.*, 1987, **8**, 257.
19 J.-P. Crocombette and L. Proville, *Appl. Phys. Lett.*, 2011, **98**, 191905.
20 F. L. Madarasz and P. G. Klemens, *Phys. Rev. B*, 1981, **23**, 2553.
21 F. Cicoira, C. Santato, F. Dinelli, M. Murgia, M. A. Loi, F. Biscarini, R. Zamboni, R. Heremans and M. Muccini, *Adv. Funct. Mater.*, 2005, **15**, 375.
22 J. M. O. Zide, D. Vashaee, Z. X. Bian, G. Zeng, J. E. Bowers, A. Shakouri and A. C. Gossard, *Phys. Rev. B.*, 2006, **74**, 205335.
23 S. Dhara, H. S. Solanki, A. P. R. V. Singh, S. Sengupta, B. A. Chalke, A. Dhar, M. Gokhale, A. Bhattacharya and M. M. Deshmukh, *Phys. Rev. B.*, 2011, **84**, 121307.
24 F. Murphy-Armando and S. Fahy, *J. Appl. Phys.*, 2011, **109**, 113703.
25 J. Martin, L. Wang, L. Chen and G. S. Nolas, *Phys. Rev. B.*, 2009, **79**, 115311.
26 B. R. Nag, *Electron Transport in Compound Semiconductors*, Springer-Verlag, New York, 1980.
27 J. Callaway, *Phys. Rev.*, 1958, **113**, 1046.
28 C. M. Bhandari and D. M. Rowe, *J. Phys. C: Solid State Phys.*, 1979, **12**, L883.
29 S. Iwanaga and G. J. Snyer, *J. Electron. Mater.*, 2012, **41**, 1667.

